Volume 10 | Number 39 | 21 October 2019 | Pages 8897–9154

Chemical Science

rsc.li/chemical-science

ISSN 2041-6539

ROYAL SOCIETY OF CHEMISTRY | Celebrating IYPT 2019

EDGE ARTICLE
José L. Mascareñas, Javier Montenegro *et al.*
Supramolecular caging for cytosolic delivery of anionic probes

Chemical Science

EDGE ARTICLE

View Article Online
View Journal | View Issue

Cite this: *Chem. Sci.*, 2019, **10**, 8930

All publication charges for this article have been paid for by the Royal Society of Chemistry

Received 13th June 2019
Accepted 19th August 2019

DOI: 10.1039/c9sc02906k

rsc.li/chemical-science

Supramolecular caging for cytosolic delivery of anionic probes†

Héctor Fernández-Caro, [a] Irene Lostalé-Seijo, [a] Miguel Martínez-Calvo, [a] Jesús Mosquera, [b] José L. Mascareñas *[a] and Javier Montenegro *[a]

The cytosolic delivery of hydrophilic, anionic molecular probes and therapeutics is a major challenge in chemical biology and medicine. Herein, we describe the design and synthesis of peptide–cage hybrids that allow an efficient supramolecular binding, cell membrane translocation and cytosolic delivery of a number of anionic dyes, including pyranine, carboxyfluorescein and several sulfonate-containing Alexa dyes. This supramolecular caging strategy is successful in different cell lines, and the dynamic carrier mechanism has been validated by U-tube experiments. The high efficiency of the reported approach allowed intracellular pH tracking by exploiting the ratiometric excitation of the pyranine fluorescent probe.

Introduction

Hydrophilic anionic small molecules and biopolymers are highly valuable intracellular probes and therapeutics.[1–5] This is the case of important fluorophores like fluorescein and sulfonated Alexas, or molecules like pyranine, a trisulfonated pyrene that presents very appealing pH-sensitive fluorescence.[6,7] Unfortunately, these dyes cannot be efficiently transported across cell membranes, mainly because of their negative charge at physiological pH (Fig. 1a).[6–12] Most strategies to promote the intracellular uptake of small anionic molecules involve a transitory reduction of charge, usually by esterification of anionic carboxylates or phosphates,[1,4,12] but this requires a covalent modification of the probe and the subsequent intracellular cleavage of the appendage. Furthermore, in the case of the sulfonated derivatives (Fig. 1a), which are very appealing from the biophysical perspective,[13] covalent esterification is synthetically difficult and cannot be implemented in cell assays.[14–16]

Alternative delivery strategies involving electrostatic trapping of the molecules within cationic amphiphiles have been essentially limited to nucleic acid cargoes.[17,18] Supramolecular tactics[3,19,20] and macrocyclic capsules such as cyclodextrins and cucurbiturils have also been used as vehicles for cell delivery of suitable guests,[21] and fluorescent probes.[22–25] However, these approaches have been mainly used for transporting hydrophobic molecules and present serious drawbacks associated with the endosomal entrapment of the cargo.[21,26] Cell-penetrating peptides have also been used for fluorophore delivery,[24,25] but in most cases the cargo is covalently linked to the peptide.[27,28] Therefore, the cargo's final destination is intrinsically connected to the penetrating peptide vehicle. Cytosolic anionic probe loading has also been attempted by physical methods, such as microinjection, strong hypotonic stress at high probe concentrations,[29] or by using pH or redox-responsive encapsulating vesicles.[7,10,30] However these methods sometimes require specific technical equipment and are limited to particular cell lines, and also suffer from endosomal entrapment of the cargo. Current strategies for the intracellular cytosolic delivery of anionic

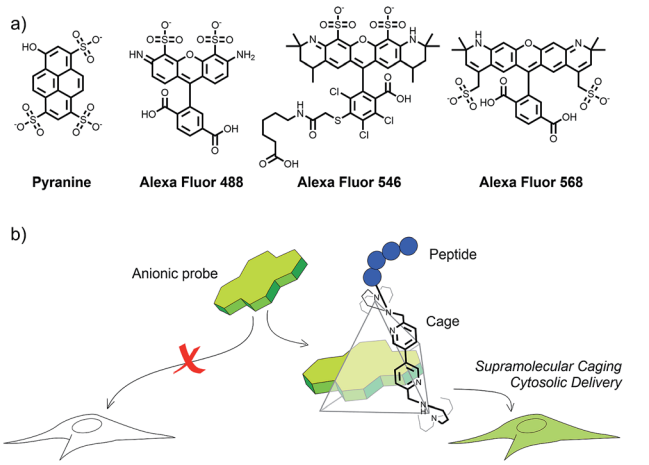

Fig. 1 (a) Examples of important fluorescent probes that do not cross cell membranes at low micromolar concentration. (b) This work: a designed covalent hybrid between tetraarginine (blue spheres) and a positively charged supramolecular cage is capable of delivering planar anionic probes into living cells, and release them from endosomes.

[a]Centro Singular de Investigación en Química Biolóxica e Materiais Moleculares (CIQUS), Departamento de Química Orgánica, Universidade de Santiago de Compostela, 15782, Santiago de Compostela, Spain. E-mail: joseluis.mascarenas@usc.es; javier.montenegro@usc.es

[b]CIC biomaGUNE, Paseo Miramón 182, 20014, Donostia/San Sebastián, Spain

† Electronic supplementary information (ESI) available: Detailed synthetic procedures and Fig. S1–S26. See DOI: 10.1039/c9sc02906k

fluorescent probes are laborious, not practical and strongly inefficient.

Therefore, there is a clear need for conceptually new methodologies for the efficient cytosolic delivery of anionic probes. Herein we present a solution to this challenge based on the temporary encapsulation of these probes into positively charged nitrogenated cages containing short cationic peptide pendants (Fig. 1b). These supramolecular conjugates behave as "truck and release" carriers and allow efficient cytosolic accumulation of a variety of anionic fluorescent cargoes that otherwise cannot be internalized and released. We have also investigated the transport mechanism and demonstrated an important application of the strategy to track the intracellular pH by using the ratiometric excitation of the pyranine probe.

Results and discussion

The cage hybrids used in our study are inspired by the pioneering work of Nitschke and coworkers who synthesized a tris-bipyridyl structure **C** that can trap pyranine molecules with high affinity in the aqueous environment (Fig. 2).[31] Indeed, this host–guest interaction has been successfully used as a switch to control the cellular uptake of peptides[32] and of gold nanoparticles previously decorated with pyranine moieties.[33] Therefore, we wondered whether supramolecular caging could be used for the cellular transport and the cytosolic delivery of planar anionic probes such as pyranine and/or sulfonated Alexa dyes, owing to the charge neutralization that should occur upon encapsulation.

Intracellular delivery of pyranine

Initial experiments were carried out using different concentrations of the cage **C**, in HeLa cells. No intracellular fluorescence was observed, which confirmed that this cationic host alone was unable to promote the intracellular transport of pyranine (5 μM, Fig. 3a and S3†). This is likely associated with the very poor internalization ability of the cage alone.[32]

Therefore, we decided to covalently attach different positively charged peptide pendants to one of the vertices of this cage in order to facilitate intracellular delivery (Fig. 2, S1 and S2†). Tagging of the cage with peptide pendants was carried out using standard conditions for amide bond formation, and the peptide–cage vectors were purified and characterized by HPLC-MS (one peptide per cage, see the ESI†). Attachment of octarginine ($\boldsymbol{R}_8$) and medium-length amphiphilic peptides like **A**, produced peptide–cage hybrids ($^{\mathbf{Tm}}\boldsymbol{R}_8\mathbf{C}$, $^{\mathbf{Tm}}\mathbf{AC}$, superindex **Tm** refers to peptides containing a TAMRA fluorophore at the N-terminus) that aggregated in the presence of pyranine, and showed toxicity and membrane damage at 5 μM in HeLa cells (Fig. S4†). The strongly cationic and amphiphilic character of these cage hybrids could explain the higher toxicity in comparison to their unmodified counterparts. However, modification of the cage **C** with tetraarginine ($\boldsymbol{R}_4$) afforded a peptide–cage conjugate ($\boldsymbol{R}_4\mathbf{C}$) with excellent aqueous solubility and cell biocompatibility at 5 μM (Fig. S5†). HPLC-MS analysis confirmed that the cage is attached to a single peptide (Fig. S23–S26†).

We thus prepared two $\boldsymbol{R}_4$-cage hybrids to study the delivery of pyranine: $^{\mathbf{Ac}}\boldsymbol{R}_4\mathbf{C}$ and $^{\mathbf{Tm}}\boldsymbol{R}_4\mathbf{C}$ (super indexes: **Ac** for the acetylated

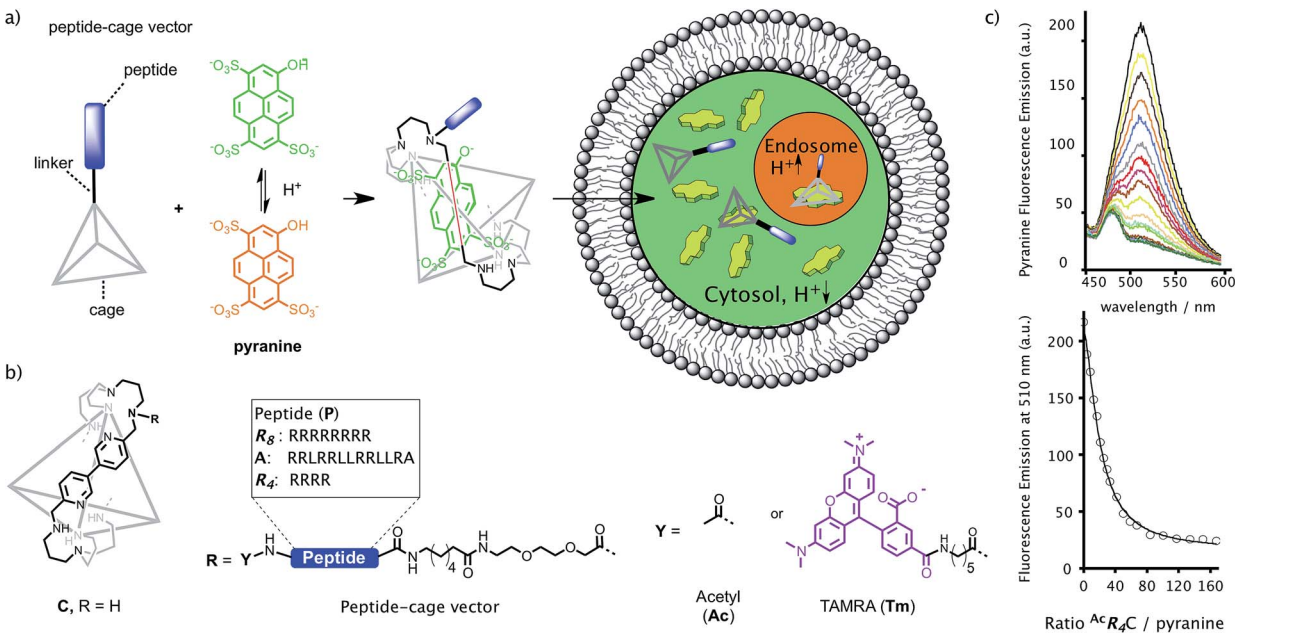

Fig. 2 (a) Cage-mediated cytosolic delivery: the peptide–cage vector recognizes pyranine, promotes its membrane translocation, and releases the cargo into the cytosol of cells. In the cage/probe complex bipyridine has been substituted with a red line for clarity. The pH dependent excitation maxima can be used to track the intracellular pH (*i.e.* endosome). (b) Structure of the peptide cage hybrids. (c) Titration of pyranine (8.4 nM) with increasing concentrations of peptide–cage $^{\mathbf{Ac}}\boldsymbol{R}_4\mathbf{C}$, showing the decrease of fluorescence of the former with increasing amounts of the peptide–cage hybrid. Fitting of the fluorescence titration to a Hill model (K_D = 189 nM).

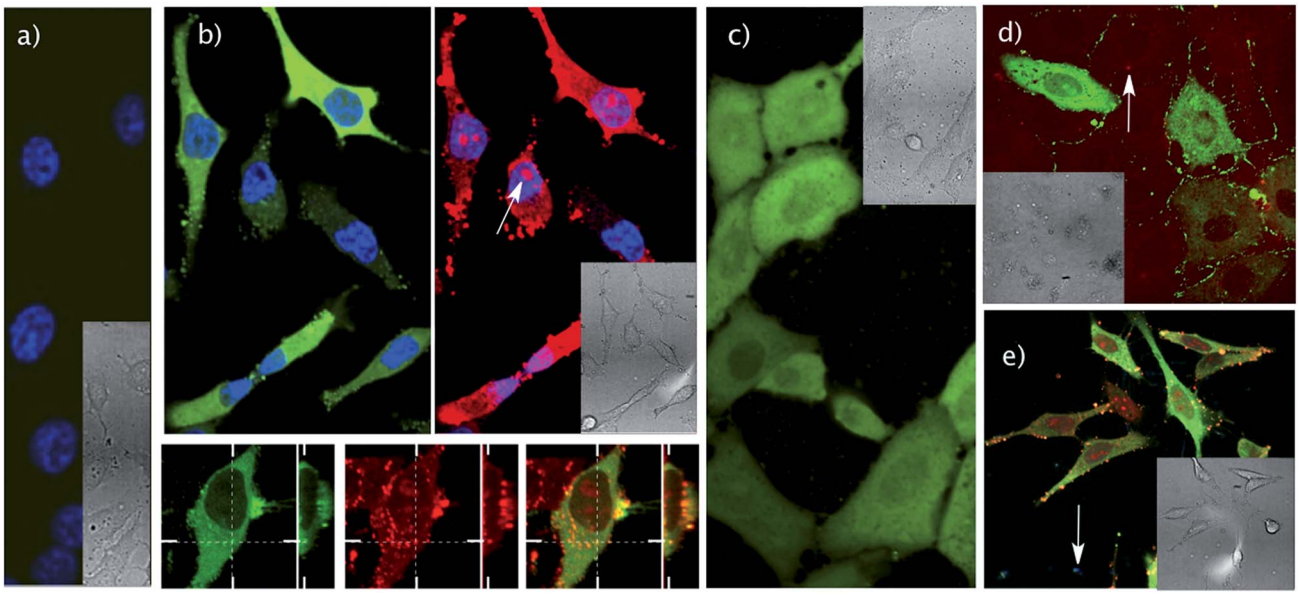

Fig. 3 Transport experiments in cells. (a) Control experiments in HeLa cells showing confocal micrographs of cells incubated with pyranine (5 μM) and cage **C** (5 μM); nuclei stained with Hoechst (blue). (b) Top: confocal micrographs of HeLa cells incubated with both pyranine (5 μM, green) and $^{Tm}R_4C$ (5 μM, red) for 30 min in HKR buffer, and washed with HKR buffer before imaging; nuclei stained with Hoechst (blue). The arrow marks the nucleolar accumulation of the peptide–cage carrier. Bottom: confocal images and orthogonal projection of the same HeLa cells showing $^{Tm}R_4C$ (red) and pyranine (green) cytosolic distribution and partial endosomal co-localization. (c) Transport of pyranine (15 μM, green) in the presence of $^{Tm}R_4C$ (15 μM), after incubation for 30 min in Vero cells, in HKR. (d) Competition experiments (Vero cells, 30 min of incubation) for $^{Ac}R_4C$ (10 μM) combined with pyranine (20 μM, green) in the presence of TAMRA (20 μM, red). (e) Transport experiments (HeLa) of pyranine (5 μM) with $^{Tm}R_4C$ (5 μM) after 30 min, followed by several washes, and subsequent 30 min incubation with 2 μM DAPI to check membrane integrity. (d and e) Red (top) and blue (bottom) fluorescence channels for the TAMRA and DAPI respectively with pyranine (green in both cases). Arrows indicate residual (red (top) and blue (bottom)) fluorescence. Insets show differential interference contrast (DIC) images. Excitation and emission wavelengths: DAPI and Hoechst: $\lambda_{exc} = 405$ nm and $\lambda_{em} = 450/50$ nm; pyranine: $\lambda_{exc} = 488$ nm and $\lambda_{em} = 525/50$ nm; TAMRA: $\lambda_{exc} = 561$ nm and $\lambda_{em} = 620/60$ nm.

hybrid and **Tm** for the TAMRA labelled derivative, Fig. 2b and S2†). Gratifyingly, titration experiments of the pyranine fluorophore with increasing concentrations of the peptide cage hybrids (*i.e.* $^{Ac}R_4C$), in phosphate buffer at pH 7, confirmed an excellent host/guest supramolecular recognition of the probe by the peptide–cage hybrids (Fig. 2c and S6a†).

The presence of the peptide reduced the affinity of pyranine for the cage (189 nM *vs.* 1.2 nM of the cage alone),[31] suggesting that the cationic peptide might hinder the ability of the cage to bind the anionic probe. The presence of the TAMRA moiety in $^{Tm}R_4C$ further reduced the affinity ($K_D = 12.6$ μM). This observation suggests a potential steric effect in the labelled peptide or a different supramolecular structure of the TAMRA labelled peptide–cage hybrids, as we could not detect any interaction of the cage with free TAMRA in fluorescence titrations (Fig. S11d†). Spinning disk confocal microscopy confirmed a very efficient internalization of $^{Tm}R_4C$ at low concentrations (*e.g.* 5 μM, Fig. S3d†) after 30 min of incubation. The fluorescence of the peptide–cage hybrid alone was localized in punctate compartments, the cytosol of the cell, and also accumulated in the nucleolus (Fig. S3d and S7a†), as previously observed for other arginine-rich peptides.[34] Using this concentration of the conjugate $^{Tm}R_4C$ (5 μM), we then carried out dose-response transport experiments at increasing concentrations of pyranine (Fig. S7†).

Not surprisingly, pyranine by itself or in the presence of the cage alone is unable to enter cells at low micromolar concentrations (Fig. 3a and S3†); however, we were pleased to observe that an equimolar (5 μM) co-incubation of pyranine and $^{Tm}R_4C$ with HeLa cells leads to a homogeneous distribution of the pyranine fluorescence in the cell cytosol (Fig. 3b and S7†). We could also detect a certain degree of endosomal co-localization of the pyranine with the fraction of the peptide–cage hybrid that remained in the endosomal compartments (Fig. 3b). The partial co-localization and the dynamic supramolecular nature of the carrier–cargo complex were in good agreement with the proposed mechanism of carrier/cargo complexation, membrane translocation and intracellular release. Therefore, the short arginine tail and the cationic cage work synergistically to facilitate the loading and cellular transport of the anionic cargo.

Transport experiments at low temperature and in the presence of endocytic inhibitors showed a reduction of the uptake of $^{Tm}R_4C$, with or without pyranine, indicating the relevance of energy dependent endocytosis for cell internalization (Fig. S8†). However, as previously mentioned, diffuse fluorescence of the peptide–cage hybrid was observed in the cytosol and also accumulated in the nucleolus of the cell (Fig. 3b and S7†). Therefore, despite the presumable endocytic uptake mechanism, the peptide–cage hybrid, with and without pyranine, was able to reach, at least in part, the cytosol of the cell. As shown in

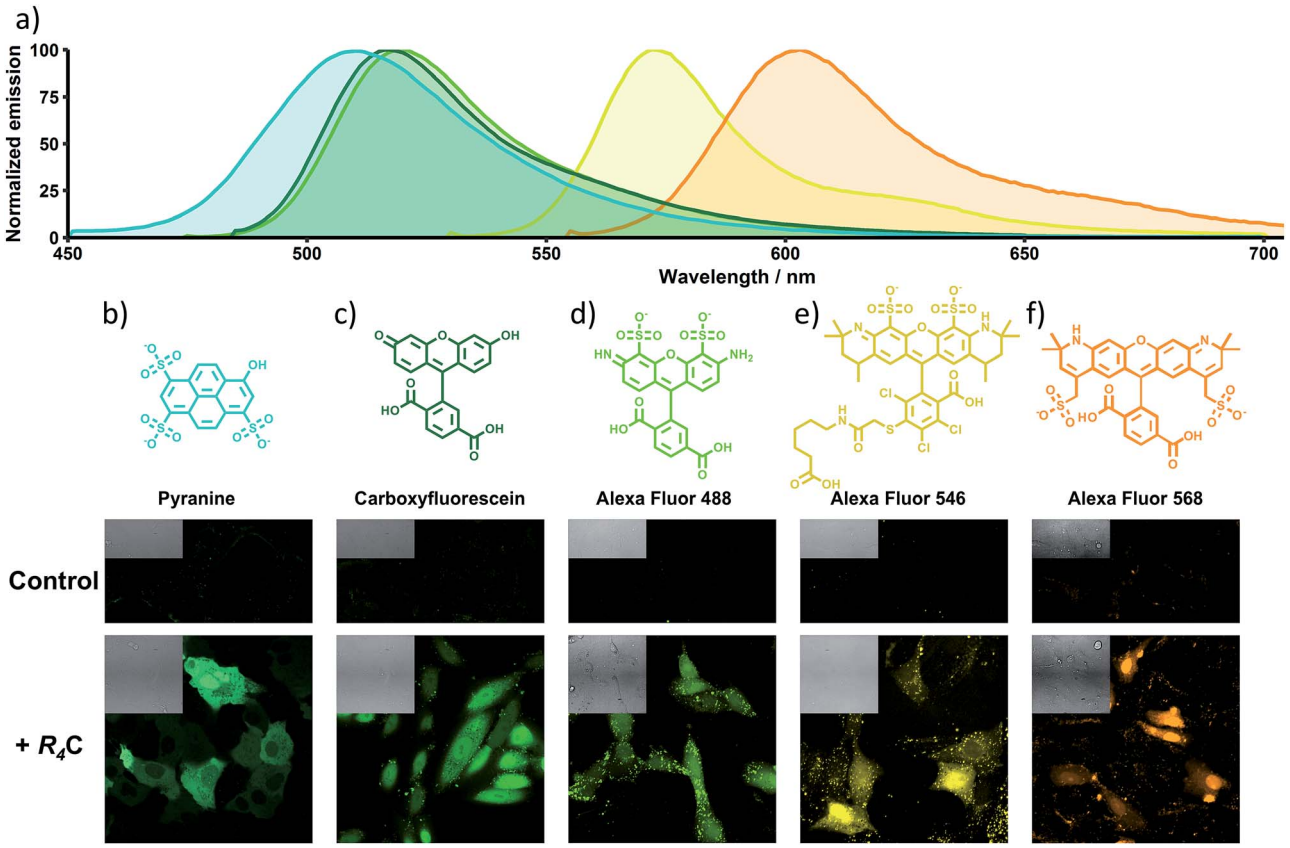

Fig. 4 Transport experiments of several anionic dyes into Vero cells. (a) Emission wavelengths of the different fluorophores. (b to f) Chemical structures and pseudocolored micrographs of Vero cells incubated for 30 min with the compounds indicated, diluted in HKR. (b) Pyranine (10 μM) and $^{Tm}R_4C$ (10 μM). (c) CF (10 μM) and $^{Tm}R_4C$ (10 μM). (d) Alexa Fluor 488 (20 μM) and $^{Tm}R_4C$ (10 μM). (e) Alexa Fluor 546 (35 μM) and $^{Ac}R_4C$ (15 μM). (f) Alexa Fluor 568 (25 μM) and $^{Ac}R_4C$ (15 μM). In all cases, control panels show the incubation of the cells with the same amount of dye in the absence of the peptide–cage hybrid. Insets show DIC images. Excitation and emission wavelengths: pyranine, CF, and Alexa Fluor 488: λ_{exc} = 488 nm and λ_{em} = 525/50 nm; Alexa Fluor 546 and Alexa Fluor 568: λ_{exc} = 561 nm and λ_{em} = 620/20 nm.

Fig. 3c, the delivery strategy can be used with different cell lines (*e.g.* Vero cells) with similar efficiency. The acetylated version of the peptide–cage hybrid ($^{Ac}R_4C$) also delivered the pyranine probe into the cytosol of HeLa and Vero cells (Fig. S7e and S9c, d†). Although the acetylated peptide could not be tracked by microscopy, the similar fluorescence patterns of the delivered probe for the TAMRA labelled and the acetylated peptide–cage hybrids suggest a similar internalization mechanism.

Cytotoxicity studies using MTT assays confirmed excellent cell viability under the conditions employed in the transport experiments (*e.g.* 5 μM peptide–cage and pyranine, Fig. S10†). Higher concentrations of the peptide–cage hybrid (*e.g.* 20 μM) in the absence of pyranine raised certain cytotoxicity, albeit this toxicity was reduced when co-incubated with the anionic pyranine cargo (Fig. S5 and S10†). This observation suggests that decreasing the cationic character of the peptide–cage carrier by supramolecular encapsulation of pyranine leads to more biocompatible and less toxic derivatives (Fig. S10†). It is worth noting that in all the above transport experiments the cell membrane keeps its integrity, as further confirmed by subsequent treatment with DAPI and propidium iodide (Fig. 3e and S9†). As expected, the cationic probe DAPI neither interacts nor is internalized by the peptide–cage hybrids. Also importantly, control transport experiments using the tetra-arginine peptide ($^{Tm}R_4$) or the cage (**C**), instead of the hybrid, did not promote any pyranine internalization (Fig. 3a and S3†).

Competition experiments by co-incubation of this acetylated peptide–cage $^{Ac}R_4C$ (10 μM) with pyranine and TAMRA (20 μM each), a fluorophore that does not show interaction with the cage at the concentrations tested (Fig. S11D†), confirmed the exclusive cytosolic delivery of pyranine (green fluorescence) but not TAMRA (red fluorescence) after 30 min of simultaneous incubation in the presence of both probes (Fig. 3d and S11†). This result further confirms that the intracellular delivery of pyranine by the peptide–cage hybrid is not due to an uncontrolled permeabilization of the plasma membrane and requires selective interaction of the fluorophore with the cage.

Delivery of different anionic fluorophores

The above-mentioned cellular transport also applies to other planar/anionic fluorescent probes such as carboxyfluorescein (CF, Fig. 4 and S12†), which is also encapsulated by the cage (Fig. S13†). Importantly, we further validated the scope of the approach by using three different sulfonate-containing Alexa

Fluor dyes, which exhibit different emission colours (λ_{exc} = 488, 546 and 568 nm). While these fluorophores are unable to enter the cells alone, they are efficiently delivered into the cytosol of the cells when the cage-peptide carrier was added to the milieu (Fig. 4). *In vitro* titration assays confirmed that the probes also bind to the peptide-containing cage (Fig. S14†).

U-tube experiments

To obtain further information on the delivery mechanism, we performed transport experiments in a U-tube, as this assay unambiguously reports on the presence of molecular carriers (Fig. 5).[35,36] Briefly, $CHCl_3$ was placed at the bottom of the U-tube, and two aqueous (*cis* and *trans*) buffers were deposited at both sides of the tube. The peptide–cage transporter was then combined with its cargo (pyranine) and with an anionic lipid (egg yolk phosphatidylglycerol, EYPG) that acts as the physiological counterion.[35,36] In this type of assay, guanidinium-rich transporters can dynamically exchange counterions to behave as hydrophilic or hydrophobic molecules in different environments. Therefore, the mixture was then placed in the *cis* buffer, the $CHCl_3$ layer was carefully stirred, and aliquots of the *trans* buffer were collected at different time points to quantify the potential anion transference across the $CHCl_3$ hydrophobic phase (see the ESI†). These experiments confirmed the enhanced transference of pyranine across the bulk phase in the presence of the peptide–cage carrier (naked eye observation, Fig. 5a), compared to the controls using only pyranine, the cage (**C**) or the tetraarginine peptide ($^{Ac}\boldsymbol{R_4}$) (Fig. 5b and S15†).[35] The strongly enhanced pyranine transport of the peptide–cage hybrid ($^{Ac}\boldsymbol{R_4}$**C**) compared to the acetylated peptide without a cage ($^{Ac}\boldsymbol{R_4}$) indicates that beyond electrostatics, the supramolecular interaction between the cage and cargo is critical for the carrier mechanism (Fig. 5b).

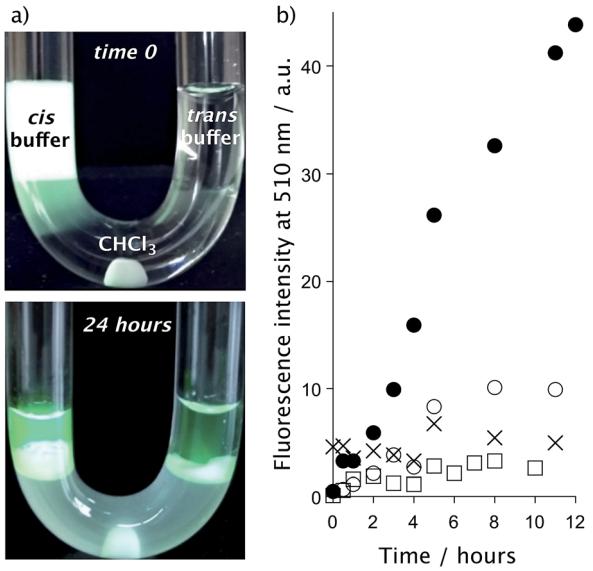

Fig. 5 U-tube transport experiments. (a) Pictures at time 0 and after 24 hours. (b) Transport of pyranine from the *cis* buffer (0.5 mL, $^{Ac}\boldsymbol{R_4}$**C**: 80 μM, EYPG: 10 mM and pyranine: 200 μM) into the *trans* buffer (0.5 mL) across the chloroform phase (1 mL) as a function of time. Buffer: 10 mM $Na_mH_nPO_4$, 100 mM NaCl, pH 7.4. Pyranine + $^{Ac}\boldsymbol{R_4}$**C** (●), pyranine + $^{Ac}\boldsymbol{R_4}$ (○), pyranine + **C** (□), pyranine (×).

Live cell pH measurements

The regulation of intracellular pH is essential to maintain cellular functions, and its alterations have been associated with diseases.[37] Therefore, diverse fluorescent sensors for the measurement of pH in different compartments of living cells have been developed, from small molecules and pH-sensitive fluorescent proteins[38] to more complex structures such as nanocapsules[39] or DNA nanomachines.[40] However, the delivery of these probes into the desired compartment is problematic, which strongly hinders the required homogeneous intracellular distribution of the probe. Pyranine has two pH-dependent excitation maxima at 405 nm (*protonated*) and 450 nm (*deprotonated*)[6] and might thus be used for intracellular ratiometric pH tracking (Fig. 2a and 6), with a pK_a that makes it especially suitable for cytosolic pH measurements. Indeed, incubation of Vero cells with $^{Tm}\boldsymbol{R_4}$**C** and pyranine (10 μM each, 30 min) allowed the straightforward differentiation of the neutral cytosol and the acidic organelles (Fig. 6b and c). Furthermore, ratiometric analysis of intracellular pyranine, after suitable pH calibration in nigericin-clamped cells (Fig. S16 and S17†), validated the excellent ratiometric pH intracellular mapping with spatiotemporal resolution (Fig. 6d). This method allowed the precise discrimination of the neutral pH of cytosol (~7.5), the slightly acidic pH of the early endosomes (~7.0) and the more acidic pH of late endosomes (~6.5).

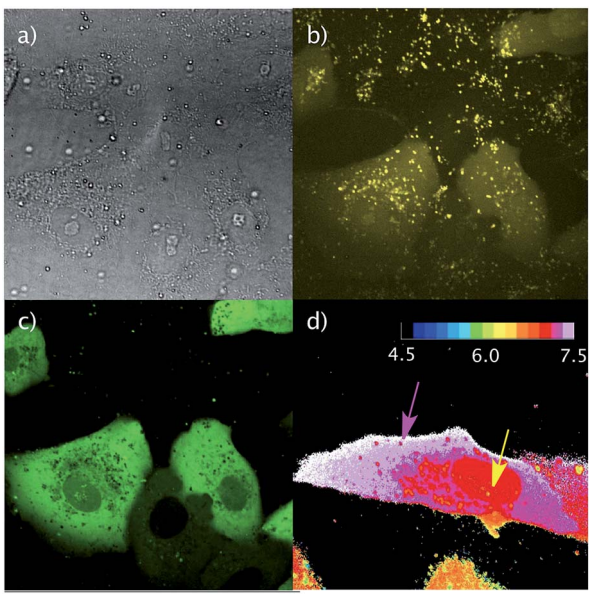

Fig. 6 Intracellular pH tracking in Vero cells. Confocal micrographs of cells incubated with pyranine (10 μM) and $^{Tm}\boldsymbol{R_4}$**C** (10 μM) for 30 min in HKR buffer. (a) DIC. (b) Channel (λ_{exc} = 405 nm and λ_{em} = 525/50 nm) corresponding to the *"protonated form"* showing higher intensity in the endosomes. (c) Channel (λ_{exc} = 488 nm and λ_{em} = 525/50 nm) corresponding to the *"deprotonated form"* showing higher cytosolic intensity. (d) Ratiometric images of Vero cells after cell calibration. Arrows: purple (early endosomes) and yellow (late endosomes).

Conclusions

In summary, this work demonstrates that cationic cages capable of hosting anionic dyes can be converted into highly efficient cellular transporters of these otherwise non-penetrating compounds, when the cages are covalently linked to a tetraarginine peptide. The transport strategy, based on a "truck and release" concept, can be operated in different cell lines and for a palette of several planar anionic probes. The efficient loading of the cell cytosol with pyranine could also be used for ratiometric intracellular pH tracking. Our results pave the way for the efficient delivery of hydrophilic therapeutics or diagnosis probes.

Experimental

Synthesis of peptides

Peptides ^{Tm}**A**, ^{Tm}***R*$_8$**, ^{Tm}***R*$_4$** and ^{Ac}***R*$_4$** were synthesized according to classic SPPS of peptides (**Tm** stands for tetramethylrhodamine, TAMRA), by manual Fmoc solid-phase peptide synthesis on a 2-chlorotrityl chloride resin (1.14 mmol g^{-1}). The first coupling was performed in CH_2Cl_2 using DIEA as the base whereas for the following couplings HBTU as the activator, DIEA as the base, and DMF as solvent were used. The deprotection of the temporal Fmoc protecting group was performed by treating the resin with 20% piperidine in DMF. Three equivalents (0.15 mmol, 64.5 mg) of 5(6)-Carboxytetramethylrhodamine (TAMRA) were coupled with 3 equivalents of HATU and 5 equivalents of DIEA 0.2 M in DMF for 60 min. Acetylation of the N-terminal group for the preparation of ^{Ac}***R*$_4$** was performed under standard Fmoc removal conditions (20% piperidine in DMF) followed by treatment with a solution of acetic anhydride and 2,6-lutidine (1 : 1, 1 mL) for 30 min. The cleavage/deprotection step was performed by treatment of the resin-bound peptide for 2 h with the following cleavage cocktail: 900 μL TFA, 50 μL CH_2Cl_2, 25 μL H_2O and 25 μL TIS (1 mL of cocktail/40 mg resin). Peptides were precipitated with Et_2O and purified by RP-HPLC. Additional details on synthesis and characterization can be found in the ESI.†

Synthesis of peptide–cage hybrids

The cage **C** was prepared and purified following the procedure reported in the literature.[31,32] For the synthesis of the supramolecular conjugates, ^{Tm}**A**, ^{Tm}***R*$_8$**, ^{Tm}***R*$_4$** and ^{Ac}***R*$_4$** peptides were dissolved in DMF (0.1 mM, 100 μL) before HATU (1 equiv.) and DIEA (10 equiv.) were added to the solution. This solution was added to a 0.1 mM solution of the cage **C** (1 equiv.) and the reaction mixture was left stirring overnight. The resulting mixture was purified by RP-HPLC and the peptide–cage species was confirmed by mass spectrometry. Additional details on synthesis and characterization can be found in the ESI.†

Fluorescence titrations

For the spectroscopic studies, a fresh solution of the dye in phosphate buffer (10 mM, pH 7) was prepared and diluted into a quartz Hellma® fluorescence cuvette with a path-length of 14 × 10 mm (chamber volume 1.4 mL) to reduce the dye concentration to the desired concentration in phosphate buffered solution (pH 7). Measurements were performed using a Varian Cary Eclipse fluorometer using the following settings: increment, 1.0 nm; integration time, 0.2 s; excitation slit width, 5.0 nm; emission slit width, 20.0 nm. The fluorescence emissions of the titrations were plotted and fitted using nonlinear regression equations (Hill 1) to obtain the apparent K_D for each experiment. Data were fitted using nonlinear analysis with Origin 8.5 to the Hill 1 equation:

$$y = y_{max} + (y_{min} - y_{max})\frac{x^n}{k^n + x^n}$$

where y_{max} and y_{min} are the maximal and minimal fluorescence values, x is the ratio of concentrations between the indicated peptide and fluorophore, n is the Hill coefficient and k is the ratio of concentrations that correspond to the K_D. From this value, K_D is calculated using the following equation:

$$K_D = kc$$

where k is the previously calculated ratio and c is the concentration of the fluorophore. A free value for the Hill coefficient (n) was selected for most of the analysis, to account for the possibility that more than one fluorophore molecule interacts with the cage.[31] Fitting using a 1 : 1 model gave a similar K_D value.

To 1.0 mL of 8.4 nM solution of pyranine, 40 nM solution of carboxyfluorescein (CF), 30 nM solution of TAMRA, 50 nM solution of Alexa Fluor 488, 30 nM solution of Alexa Fluor 546, or 50 nM solution of Alexa Fluor 568, in phosphate buffer (10 mM, pH 7), aliquots of 19 μM stock solution of ^{Ac}***R*$_4$**C were sequentially added, and the fluorescence spectrum was recorded after each addition. Emission measurements were carried out by using an excitation wavelength of 415 nm for pyranine, 490 nm for CF, 488 nm for Alexa Fluor 488, and 520 nm for TAMRA, Alexa Fluor 546 and Alexa Fluor 568. The emission spectra were recorded at room temperature from 450 to 600 nm for pyranine, from 495 to 700 nm for CF and Alexa Fluor 488, and from 525 to 700 nm for TAMRA, Alexa Fluor 546 and Alexa Fluor 568. The fluorescence emission maxima of the titrations, at 510 nm for pyranine, at 516 nm for CF, at 513 nm for Alexa Fluor 488, at 570 nm for Alexa Fluor 546 and at 603 nm for Alexa Fluor 568, were plotted and fitted using nonlinear regression equations (Hill 1) to achieve the apparent K_D for each experiment. For titrations with ^{Tm}***R*$_4$**C, to a 60 nM solution of pyranine or a 40 nM solution of CF, aliquots of 19 μM stock solution of the peptide were sequentially added and the spectra were recorded under the same conditions described for ^{Ac}***R*$_4$**C.

U-tube experiments

U-tube experiments were carried out following previously described procedures[35] with minimal modifications. The *cis* phase (0.46 mL; 0.200 mM pyranine, 10 mM $Na_mH_nPO_4$, 100 mM NaCl, pH 7.4) containing additional solution of EYPG (10 mM) was vortexed with $CHCl_3$ (0.5 mL). Then, 40 μL of ^{Ac}***R*$_4$**C, 40 μL of ^{Ac}***R*$_4$** or 40 μL of **C** of a 1 mM aqueous solution

were added, and the mixture was vortexed again. Both the organic and aqueous layers were added carefully to the U-tube containing $CHCl_3$ (1 mL) and the *trans* phase (0.5 mL) from the sampling side. The organic layer was stirred at 700 rpm at room temperature. Aliquots (13.5 μL) were taken from the *trans* phase as a function of time and diluted to 150 μL with a buffer (10 mM $Na_mH_nPO_4$, 100 mM NaCl, pH 7.4). Measurements were performed using a Varian Cary Eclipse fluorometer with the following settings: integration time, 0.2 s; excitation slit width, 5.0 nm; emission slit width, 20.0 nm; excitation wavelength, 460 nm. The emission spectra were recorded from 470 to 600 nm at 20 °C.

Cell lines and culture

HeLa (ATCC) and Vero (ATCC) cell lines were maintained at 37 °C, 5% CO_2, 95% humidity, in Dulbecco's Modified Eagle's Medium (4500 mg L^{-1} glucose, L-glutamine, sodium pyruvate and sodium bicarbonate), supplemented with 10% fetal bovine serum and 1% of Penicillin–Streptomycin–Glutamine mix, and kept in an INCO108 incubator (Memmert).

Cell transport experiments

HeLa or Vero cells seeded the day before on glass-bottom dishes were washed with HEPES-Krebs-Ringer (HKR) buffer (5 mM HEPES, 137 mM NaCl, 2.68 mM KCl, 2.05 mM $MgCl_2$, 1.8 mM $CaCl_2$, pH 7.4) and incubated for 30 min with 1 μM Hoechst 33342 (ThermoFisher) in HKR to stain the nucleus. This solution was removed and cells were incubated for another 30 min with pyranine (or other fluorescent probes such as TAMRA, CF or Alexa Fluor dyes) in combination with the peptide, cage or peptide–cage hybrids at the concentrations indicated in the legend of the figures. After this incubation time, cells were washed twice with HKR and examined on the confocal microscope. In some cases, the step of nuclear staining with Hoechst was omitted. To check membrane integrity, after incubation with the complexes, cells were washed with HKR and further incubated with 2 μM of DAPI diluted in HKR buffer for 30 min or 0.5 μg mL^{-1} of propidium iodide for 10 min, before washing with HKR and imaging. To investigate the possibility of the *in situ* capture of pyranine into the cage of the carrier, Vero cells were incubated with 12.5 μM pyranine in HKR for 10 min before adding dropwise a solution of $^{Ac}\boldsymbol{R_4}$**C** in HKR to a final concentration of both the peptide and pyranine of 10 μM and incubated for 30 min at 37 °C before imaging.

In vitro pH measurements

To confirm pH sensitivity of the dye in the calibration buffers used for *in situ* calibration (10 mM MES, 10 mM HEPES, 20 mM glucose, 1 mM $CaCl_2$, 1 mM $MgCl_2$, 135 mM KCl, 20 mM NaCl; pH adjusted with KOH), absorption spectra of pyranine in the different buffers were obtained. Pyranine was diluted at 70 μM in each buffer and absorbance between 330 and 510 nm was measured using a Libra S60 spectrophotometer. Ratios between absorbance at 450 and 405 nm were calculated and then transformed using the following equation:

$$\log_{10}\left(\left(\frac{R_{max}-R}{R-R_{min}}\right)\left(\frac{A^{basic}_{405\ nm}}{A^{acidic}_{405\ nm}}\right)\right)$$

where R represents the ratio A_{450}/A_{405}, R_{max} and R_{min} are the maximal and minimal ratio values, and A^{basic}_{405} and A^{acidic}_{405} are the absorbance of pyranine at the highest and lowest pH tested. Data were fitted to a linear model. The intercept (7.01) corresponds to the pK_a under these conditions.

pH studies of cells

For pH ratiometric measurements, Vero cells were incubated with 10 μM pyranine and 10 μM $^{Tm}\boldsymbol{R_4}$**C** peptide for 30 min in HKR buffer. The cells were then washed twice with HKR and imaged. A control with no pyranine was also prepared to quantify the background. To prepare a calibration curve, cells were first incubated with pyranine and $^{Tm}\boldsymbol{R_4}$**C** under standard conditions (30 min, pH = 7.4). Subsequently, the cells were washed twice with high-potassium pH calibration buffers (10 mM MES, 10 mM HEPES, 20 mM glucose, 1 mM $CaCl_2$, 1 mM $MgCl_2$, 135 mM KCl, 20 mM NaCl; pH adjusted with KOH) at each indicated pH. The cells were then incubated at the corresponding pH for 20 min with the calibration buffers containing 10 μg mL^{-1} of the ionophore nigericin for pH clamping before imaging. Images were acquired with a Zyla 4.2 PLUS camera mounted on a Dragonfly spinning disk confocal microscope (Andor), by excitation with 405 nm (protonated form, PyrH) and 488 nm (deprotonated form, Pyr^-) lasers, detecting the fluorescence at 500–550 nm. Images from the pyranine channels were processed with FIJI,[41] as follows: the background was subtracted from both channels and then the image 488 was divided by the image 405. Mean values per field were obtained (Fig. S17b†) and data were linearized by logarithmic conversion and adjusted to a linear model (Fig. S17c†). The linear fit was then used to assign estimated values of pH to the images.

Flow cytometry

In order to further investigate the uptake mechanisms of the supramolecular complex formed by $^{Tm}\boldsymbol{R_4}$**C** and pyranine, Vero cells seeded the day before at 10.000 cells per well on a 96-well plate were treated for 30 min with dynasore (80 μM) diluted in DMEM without serum or antibiotics. The cells were then washed with HKR and incubated with 15 μM $^{Tm}\boldsymbol{R_4}$**C** and 15 μM pyranine during 30 min at 37 °C with the same concentration of the inhibitor in HKR buffer. For the incubation at low temperature (4 °C), the cells were placed on ice before the incubation, and ice-cold solutions were used for the washes and incubations. Controls with 15 μM $^{Tm}\boldsymbol{R_4}$**C** alone and 15 μM pyranine alone were also performed. After 30 min of incubation, the cells were washed with HKR and trypsinized. Trypsin was neutralized with 2% FBS in PBS with 5 mM EDTA and cell fluorescence was measured on a Guava EasyCyte™ cytometer using two lasers: a blue laser (488 nm) with emission collected at 512/18 nm (pyranine) and a green laser (532 nm) collecting the emission at 575/25 nm (TAMRA). Cells with typical FSC and SSC parameters were selected and the median fluorescence intensity (MFI) was

calculated for each sample. Each condition was performed in triplicate. Fluorescence values were normalized to the uptake of each untreated control (100%) after blank subtraction. In all cases, data analysis was performed with InCyte software included in GuavaSoft 3.2 (Millipore).

Cell viability

Cell viability was measured by MTT assays. To evaluate the toxicity of the treatment of cells with $^{Tm}\boldsymbol{R}_4\mathbf{C}$, $^{Ac}\boldsymbol{R}_4\mathbf{C}$ and pyranine, Vero and HeLa cells were subjected to an MTT assay 1 hour and 24 h after the incubation. One day before the assay, a suspension of HeLa and Vero cells was plated in 96-well tissue culture plates by adding 100 μL (~10.000 cells) per well. Next day, the medium was removed and the cells were incubated in HKR in the presence of $^{Tm}\boldsymbol{R}_4\mathbf{C}$, $^{Ac}\boldsymbol{R}_4\mathbf{C}$, and pyranine at different concentrations (50 μL per well) during 1 hour of incubation at 37 °C. After the incubation, HKR with the compounds was removed and the pre-warmed DMEM containing 10% FBS was added to the wells. To evaluate the toxicity at 1 hour, MTT (5 mg mL^{-1} in PBS, 10 μL per well) was added and the cells were further incubated for 4 h. To evaluate the toxicity at 24 h, the cells were incubated for 24 h before adding the MTT. The cells were further incubated for 4 h in the presence of MTT. The supernatant was carefully removed and the water-insoluble formazan salt was dissolved in DMSO (100 μL per well). The absorbance at 570 nm was measured. Data points were collected in triplicate and expressed as normalized values for untreated control cells (100%) after blank subtraction.

Conflicts of interest

There are no conflicts to declare.

Acknowledgements

We acknowledge funding from the Spanish Agencia Estatal de Investigación (AEI) [CTQ2014-59646-R, SAF2017-89890-R, and SAF2016-76689-R], the Xunta de Galicia (ED431G/09, 2015-CP082, ED431C 2017/19, 2016-AD031, and Centro Singular de Investigación de Galicia accreditation 2016–2019, and ED431G/09) and the European Union (European Regional Development Fund – ERDF), and the European Research Council (Advanced Grant No. 340055 for JLM and Starting Grant for J. Montenegro (DYNAP-677786)). H. F.-C. thanks Xunta de Galicia (Predoctoral fellowship: ED481A-2017/047). J. Montenegro received a RyC (RYC-2013-13784) and a Young Investigator Grant from the HFSP (RGY0066/2017). J. M. and M. M.-C. thank MINECO for JdC fellowships (FJCI-2015-25080 and IJCI-2014-19326). We thank Prof. Jonathan R. Nitschke for assistance in the preparation of the covalent cage. We thank Rebeca Menaya-Vargas for assistance with cell culture.

Notes and references

1 B. R. Meade, K. Gogoi, A. S. Hamil, C. Palm-Apergi, A. van den Berg, J. C. Hagopian, A. D. Springer, A. Eguchi, A. D. Kacsinta, C. F. Dowdy, A. Presente, P. Lönn, M. Kaulich, N. Yoshioka, E. Gros, X.-S. Cui and S. F. Dowdy, *Nat. Biotechnol.*, 2014, **32**, 1256–1261.
2 J. A. Zuris, D. B. Thompson, Y. Shu, J. P. Guilinger, J. L. Bessen, J. H. Hu, M. L. Maeder, J. K. Joung, Z.-Y. Chen and D. R. Liu, *Nat. Biotechnol.*, 2015, **33**, 73–80.
3 J. Yang, A. Bahreman, G. Daudey, J. Bussmann, R. C. L. Olsthoorn and A. Kros, *ACS Cent. Sci.*, 2016, **2**, 621–630.
4 K. A. Mix, J. E. Lomax and R. T. Raines, *J. Am. Chem. Soc.*, 2017, **139**, 14396–14398.
5 I. Lostalé-Seijo and J. Montenegro, *Nat. Rev. Chem.*, 2018, **2**, 258–277.
6 C. C. Overly, K. D. Lee, E. Berthiaume and P. J. Hollenbeck, *Proc. Natl. Acad. Sci. U. S. A.*, 1995, **92**, 3156–3160.
7 H.-S. Chou, M.-H. Hsiao, W.-Y. Hung, T.-Y. Yen, H.-Y. Lin and D.-M. Liu, *J. Mater. Chem. B*, 2014, **2**, 6580–6589.
8 M. Fernández-Suárez and A. Y. Ting, *Nat. Rev. Mol. Cell Biol.*, 2008, **9**, 929–943.
9 B. Turkowyd, D. Virant and U. Endesfelder, *Anal. Bioanal. Chem.*, 2016, **408**, 6885–6911.
10 W. C. de Vries, D. Grill, M. Tesch, A. Ricker, H. Nüsse, J. Klingauf, A. Studer, V. Gerke and B. J. Ravoo, *Angew. Chem., Int. Ed.*, 2017, **56**, 9603–9607.
11 A. Fernandez, M. Vermeren, D. Humphries, R. Subiros-Funosas, N. Barth, L. Campana, A. MacKinnon, Y. Feng and M. Vendrell, *ACS Cent. Sci.*, 2017, **3**, 995–1005.
12 I. Johnson and M. Spence, *Molecular probes handbook: a guide to fluorescent probes and labeling technologies*, Life Technologies, Carlsbad, 11th edn, 2010.
13 J. Bishop-Stewart, M. K. Bhalgat, R. P. Haugland, P. J. Millard, N. Panchuk-Voloshina, W.-Y. Leung, R. P. Haugland and F. Mao, *J. Histochem. Cytochem.*, 2011, **47**, 1179–1188.
14 S. C. Miller, *J. Org. Chem.*, 2010, **75**, 4632–4635.
15 A. Choi and S. C. Miller, *Org. Biomol. Chem.*, 2017, **15**, 1346–1349.
16 S. M. Pauff and S. C. Miller, *Org. Lett.*, 2011, **13**, 6196–6199.
17 I. Lostalé-Seijo, I. Louzao, M. Juanes and J. Montenegro, *Chem. Sci.*, 2017, **8**, 7923–7931.
18 J. M. Priegue, D. N. Crisan, J. Martínez-Costas, J. R. Granja, F. Fernandez-Trillo and J. Montenegro, *Angew. Chem., Int. Ed.*, 2016, **55**, 7492–7495.
19 K. Petkau-Milroy, M. H. Sonntag, A. H. A. M. van Onzen and L. Brunsveld, *J. Am. Chem. Soc.*, 2012, **134**, 8086–8089.
20 G. M. Fernandes-Cunha, C. J. McKinlay, J. R. Vargas, H. J. Jessen, R. M. Waymouth and P. A. Wender, *ACS Cent. Sci.*, 2018, **4**, 1394–1402.
21 M. J. Webber and R. Langer, *Chem. Soc. Rev.*, 2017, **46**, 6600–6620.
22 S. Swaminathan, C. Fowley, B. McCaughan, J. Cusido, J. F. Callan and F. M. Raymo, *J. Am. Chem. Soc.*, 2014, **136**, 7907–7913.
23 D. A. Harrington, H. A. Behanna, G. N. Tew, R. C. Claussen and S. I. Stupp, *Chem. Biol.*, 2005, **12**, 1085–1091.
24 D. Tian, J. Zhu, P. Gao, X. Shu, Q. Zhao, K. Wang, Z. Zhu and Y. Li, *J. Am. Chem. Soc.*, 2018, **140**, 17484–17491.

25 E. Derivery, E. Bartolami, S. Matile and M. Gonzalez-Gaitan, *J. Am. Chem. Soc.*, 2017, **139**, 10172–10175.
26 D. Kalafatovic and E. Giralt, *Molecules*, 2017, **22**, 1929.
27 W. B. Kauffman, T. Fuselier, J. He and W. C. Wimley, *Trends Biochem. Sci.*, 2015, **40**, 749–764.
28 D. M. Copolovici, K. Langel, E. Eriste and Ü. Langel, *ACS Nano*, 2014, **8**, 1972–1994.
29 B. S. Gan, E. Krump, L. D. Shrode and S. Grinstein, *Am. J. Physiol.*, 1998, **275**, C1158–C1166.
30 E. Yuba, Y. Kono, A. Harada, S. Yokoyama, M. Arai, K. Kubo and K. Kono, *Biomaterials*, 2013, **34**, 5711–5721.
31 J. Mosquera, S. Zarra and J. R. Nitschke, *Angew. Chem., Int. Ed.*, 2014, **53**, 1556–1559.
32 J. Rodríguez, J. Mosquera, J. R. Couceiro, J. R. Nitschke, M. E. Vázquez and J. L. Mascareñas, *J. Am. Chem. Soc.*, 2017, **139**, 55–58.
33 J. Mosquera, M. Henriksen-Lacey, I. García, M. Martínez-Calvo, J. Rodríguez, J. L. Mascareñas and L. M. Liz-Marzán, *J. Am. Chem. Soc.*, 2018, **140**, 4469–4472.
34 R. M. Martin, G. Ter-Avetisyan, H. D. Herce, A. K. Ludwig, G. Lättig-Tünnemann and M. C. Cardoso, *Nucleus*, 2015, **6**, 314–325.
35 Previously reported U-tube assays with polyarginine peptide carriers showed that the strongly anionic pyranine was difficult to be transferred to the *trans* buffer across the chloroform phase, see: N. Sakai and S. Matile, *J. Am. Chem. Soc.*, 2003, **125**, 14348–14356.
36 T. Takeuchi, V. Bagnacani, F. Sansone and S. Matile, *ChemBioChem*, 2009, **10**, 2793–2799.
37 J. R. Casey, S. Grinstein and J. Orlowski, *Nat. Rev. Mol. Cell Biol.*, 2010, **11**, 50–61.
38 J. Han and K. Burgess, *Chem. Rev.*, 2010, **110**, 2709–2728.
39 P. Rivera-Gil, M. Nazarenus, S. Ashraf and W. J. Parak, *Small*, 2012, **8**, 943–948.
40 S. Modi, C. Nizak, S. Surana, S. Halder and Y. Krishnan, *Nat. Nanotechnol.*, 2013, **8**, 459–467.
41 J. Schindelin, I. Arganda-Carreras, E. Frise, V. Kaynig, M. Longair, T. Pietzsch, S. Preibisch, C. Rueden, S. Saalfeld, B. Schmid, J.-Y. Tinevez, D. J. White, V. Hartenstein, K. Eliceiri, P. Tomancak and A. Cardona, *Nat. Methods*, 2012, **9**, 676–682.